Magnetic properties of nanostructured $CuFe_2O_4$

1999 J. Phys.: Condens. Matter 11 4063

(http://iopscience.iop.org/0953-8984/11/20/313)

J. Phys.: Condens. Matter **11** (1999) 4063–4078. Printed in the UK PII: S0953-8984(99)99862-4

Magnetic properties of nanostructured $CuFe_2O_4$

J Z Jiang†§, G F Goya‡ and H R Rechenberg‡

† Department of Physics, Building 307, Technical University of Denmark, DK-2800, Lyngby, Denmark

‡ Instituto de Física, Universidade de São Paulo, CP 66318, 05315-970 São Paulo SP, Brazil

E-mail: jiang@fysik.dtu.dk

Received 2 December 1998

Abstract. The structural evolution and magnetic properties of nanostructured copper ferrite, $CuFe_2O_4$, have been investigated by x-ray diffraction, Mössbauer spectroscopy, and magnetization measurements. Nanometre-sized $CuFe_2O_4$ particles with a partially inverted spinel structure were synthesized by high-energy ball milling in an open container with grain sizes ranging from 9 to 61 nm. Superparamagnetic relaxation effects have been observed in milled samples at room temperature by Mössbauer and magnetization measurements. At 15 K, the average hyperfine field of $CuFe_2O_4$ decreases with decreasing average grain size while the coercive force, shift of the hysteresis loop, magnetic hardness, and saturation magnetization at 4.2 K increase with decreasing average grain size. At 295 K the coercive-field dependence on the average grain size is described, with particles showing superparamagnetic relaxation effects. At 4.2 K the relationship between the coercive field and average grain size can be attributed to the change of the effective anisotropy constant of the particles. The interface anisotropy of nanostructured $CuFe_2O_4$ is found to be about $1.8(1) \times 10^5$ erg cm^{-3}. Although spin canting was present, approximately 20% enhancement of the saturation magnetization in $CuFe_2O_4$ nanoparticles was observed, which could be explained by a cation redistribution induced by milling. The high-field magnetization irreversibility and shift of the hysteresis loop detected in our samples have been assigned to a spin-disordered phase, which has a spin-freezing temperature of approximately 50 K.

1. Introduction

Spinel ferrites and their related structures have been investigated for nearly four decades, due to their theoretical and technological relevance. A great number of methods have been successfully employed to synthesize such materials with improved properties for specific applications, such as magnetic powders for massive storage devices [1]. The use of ball milling as an alternative synthesis route has focused attention on the unusual magnetic properties arising from nanometre-sized grains, vacancy densities, and changes in site populations having their origins in the milling process [2–4]. Recently, the observed reduction of the saturation magnetization and the high-field magnetization irreversibility in ferrimagnetic nanoparticles have renewed interest in these systems [5–7]. Spin canting, defined as a lack of full alignment of the spins in magnetic particles in large applied magnetic fields, has usually been proposed to account for these observations. However, the underlying mechanism that gives rise to the spin-canting phenomenon remains unclear, despite more than twenty years of studies [6–13].

Copper ferrite, $CuFe_2O_4$, can be described as a cubic close-packed arrangement of oxygen ions, with Cu^{2+} and Fe^{3+} ions at two different crystallographic sites [14]. These sites have

§ Author to whom any correspondence should be addressed. Telephone: +45 45 25 31 65; fax: +45 45 93 23 99.

tetrahedral and octahedral oxygen coordination (A and B sites respectively), so the resulting local symmetries of the two sites are different. The cation distribution in this kind of structure may be represented by $(Cu_\delta Fe_{1-\delta})^A[Cu_{1-\delta}Fe_{1+\delta}]^B O_4$, where δ is the inversion parameter and $\delta = 0$ and 1 stand for the inverse and normal cases, respectively. Although most spinel ferrites are cubic, $CuFe_2O_4$ can have tetragonal unit-cell symmetry if the sample is slowly cooled from high temperatures [15, 16]. This material is ferrimagnetic with a Néel temperature $T_N = 780(20)$ K [15], although considerable dispersion in T_N-values is found in the literature [14]. In this work, we present a study of nanostructured $CuFe_2O_4$ obtained by mechanical milling of tetragonal $CuFe_2O_4$ ferrite in an open container. The structural and magnetic properties of the materials were investigated through x-ray diffraction (XRD), Mössbauer, and magnetization measurements. We found that the saturation magnetization increases remarkably with milling time, attaining a value approximately 20% larger than that for the bulk material. High-field magnetization irreversibility is observed in samples after field cooling (FC) at 4.2 K in fields of 80 and 90 kOe. The observation of shifts in the hysteresis loops at low temperatures indicates the presence of an exchange anisotropy in these particles, which is discussed in terms of the spin freezing of a spin-disordered phase below approximately 50 K.

2. Experimental procedure

The starting $CuFe_2O_4$ sample was prepared by dissolving metallic Fe and Cu (99.99% purity) in a diluted HNO_3 solution, to obtain a nominal composition $CuFe_2O_4$. The resulting solution was slowly heated until the solvent was completely evaporated, and the resulting mire was fired at 773 K for 12 h. Three additional heat treatments in air at 1223 K for 72 h were applied, with intermediary grindings. A cooling rate of 2 K per minute was used in the last cycle. The formation of tetragonal copper ferrite was confirmed by x-ray diffraction analysis. Nanometre-sized grains were produced from the starting $CuFe_2O_4$ powder by means of dry milling (i.e., no organic surfactant was added), carried out in an open container, by keeping the valves on the lid open during operation. A planetary ball-mill (Fritsch Pulverisette 5) with hardened steel vials and balls was used. The milling intensity was set to 200 rotations per minute, and a ball-to-powder weight ratio of 20:1 was chosen. The milling process was interrupted after selected times to take out small amounts of powder. The samples will hereafter be labelled S1, S4, S7, S13, S20, and S29, where each number indicates the milling time in hours. The composition of the sample S29 was analysed by scanning electron microscopy with an energy-dispersive x-ray analysis facility. The Cr content originating from the abrasion of the vials and balls was found to be less than 0.5 wt%. The transmission electron microscopy (TEM) measurements for S29 were carried out using a Philips EM430 TEM. All of the samples were examined by x-ray diffraction in Bragg–Brentano geometry using a Philips PW-1820/3711 diffractometer with Cu Kα radiation. The data were collected in the 2θ range of 10°–80°, in steps of 0.02°, and with a counting time of 25 seconds per step. Mössbauer measurements were performed with a conventional constant-acceleration spectrometer in transmission geometry with a source of 50 mCi ^{57}Co in a Rh matrix. All isomer shifts are given relative to that of α-Fe at room temperature. A closed-cycle helium refrigerator and a nitrogen cryostat were used for low-temperature Mössbauer measurements and an electromagnet was used for in-field Mössbauer measurements. Magnetization measurements were performed in a vibrating-sample magnetometer between 4.2 and 295 K using a superconducting magnet to produce fields up to 90 kOe. Hysteresis loops at 4.2 K were measured after field cooling the samples in fields of 80 kOe or 90 kOe.

3. Results

The x-ray diffraction pattern of the starting powder could be indexed as that of single-phase tetragonal $CuFe_2O_4$ spinel. Figure 1 shows XRD data for samples milled from 1 to 29 h together with those for the sample S29 annealed in air at 973 K for 1 h. The Bragg peaks broaden and lose intensity with milling time. After 7 h of milling, the two stronger peaks corresponding to (211) and (103) reflections at $2\theta \approx 34.7^\circ$ and 35.9°, respectively, merge into a single broad peak, indistinguishable from the strongest reflection of the cubic $CuFe_2O_4$ phase ($2\theta \approx 35.6^\circ$). This feature prevents an accurate determination of the crystal structure for milled samples from being made. However, the Bragg peak at $2\theta \approx 54^\circ$ appears in all of the XRD patterns, indicating a tetragonal structure in the milled samples since no Bragg peaks are allowed in a 2θ range of 43°–57° in the cubic $CuFe_2O_4$ phase. The average grain sizes, d, of $CuFe_2O_4$ were calculated from the broadening of the peak at $2\theta \approx 18.3^\circ$, using the Scherrer equation. The evolution of d with milling time is shown in figure 2. For S1 a value of $d = 61(5)$ nm is found, which decreases with milling time and attains a nearly constant value of 10(3) nm for samples milled for longer than 13 h. The sample S29 was subsequently annealed in air at 973 K for 1 h. From the corresponding XRD pattern (also shown in figure 1), a value of approximately 41(3) nm is deduced, and it can be observed that the original tetragonal structure is not fully recovered. No other phases are observed from these data, indicating that no chemical transformation took place during milling or after the heat treatment. TEM measurements of S29 revealed large agglomerations of particles with an average grain size of approximately 10 nm.

The Mössbauer spectrum of the starting tetragonal $CuFe_2O_4$ is composed of two magnetic sextets (M1 and M2) with hyperfine fields $B = 51.0$ and 48.2 T at 295 K, corresponding to octahedral and tetrahedral sites, respectively [15, 17, 18]. Mössbauer spectra recorded at 295 K for milled samples are shown in figure 3, and the corresponding fitted parameters in table 1. It can be seen that the M1 and M2 magnetic sextets, corresponding to bulk $CuFe_2O_4$, are present in all milled samples and that their relative area decreases from 96.1% of the total resonant signal for S1 to 37.3% for S29 while their hyperfine fields also decrease with milling time.

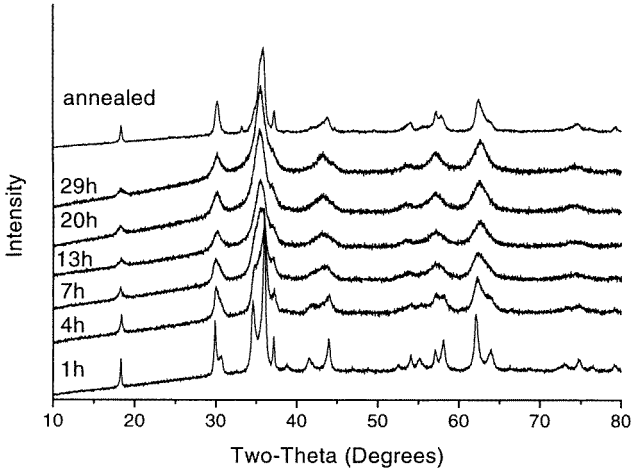

Figure 1. X-ray diffraction patterns of the $CuFe_2O_4$ samples after different milling times together with that of the sample S29 annealed in air at 973 K for 1 h.

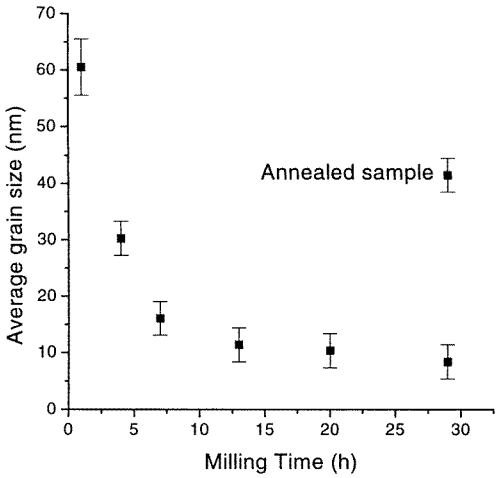

Figure 2. The average grain size of $CuFe_2O_4$, estimated from the broadening of the diffraction peak at $2\theta \approx 18.3^\circ$ using the Scherrer method, as a function of the milling time together with that of the sample S29 annealed in air at 973 K for 1 h.

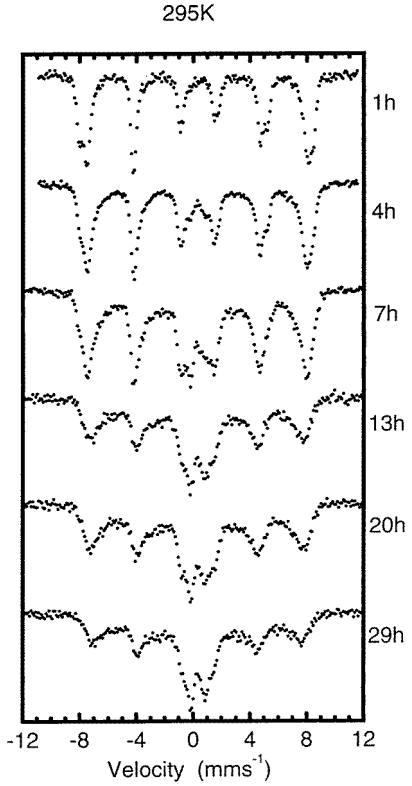

Figure 3. Mössbauer spectra recorded at 295 K for $CuFe_2O_4$ samples with various milling times.

For milling times $t \geqslant 4$ h, a third sextet M3 develops (see table 1) with a relative area of approximately 25–35% of the total resonant area. The low hyperfine field and large linewidth of the magnetic subspectra suggest a significant degree of magnetic relaxation and/or magnetic

Table 1. Mössbauer parameters: hyperfine field (B), isomer shift (δ), quadrupole splitting (Δ), linewidth (Γ), and relative area (A), obtained by fitting the spectra recorded at 295 K for the $CuFe_2O_4$ samples milled for various times.

Milling time (h)	Parameters	M1	M2	M3	P1	P2
1	B (T)	50.9	48.1		0.0	
	δ (mm s^{-1})	0.37	0.27		0.42	
	Δ (mm s^{-1})	−0.16	−0.01		1.36	
	Γ (mm s^{-1})	0.47	0.59		0.99	
	A (%)	33.9	62.2		3.9	
4	B (T)	50.4	47.8	43.0	0.0	0.0
	δ (mm s^{-1})	0.39	0.27	0.38	0.39	0.28
	Δ (mm s^{-1})	−0.14	−0.03	−0.03	1.34	0.99
	Γ (mm s^{-1})	0.54	0.59	1.92	0.85	1.25
	A (%)	21.9	41.4	25.9	4.3	6.5
7	B (T)	49.8	47.6	42.1	0.0	0.0
	δ (mm s^{-1})	0.39	0.28	0.36	0.40	0.20
	Δ (mm s^{-1})	−0.11	0.01	−0.02	1.43	0.91
	Γ (mm s^{-1})	0.65	0.73	2.55	1.24	1.08
	A (%)	12.4	32.0	34.7	11.4	9.6
13	B (T)	47.5	44.2	33.4	0.0	0.0
	δ (mm s^{-1})	0.29	0.32	0.40	0.37	0.30
	Δ (mm s^{-1})	−0.05	−0.02	−0.04	1.50	0.96
	Γ (mm s^{-1})	0.69	1.45	3.21	1.73	0.62
	A (%)	15.4	31.5	23.7	17.8	11.6
20	B (T)	47.7	43.9	−33.0	0.0	0.0
	δ (mm s^{-1})	0.32	0.30	0.34	0.43	0.29
	Δ (mm s^{-1})	−0.02	−0.01	−0.04	1.60	0.92
	Γ (mm s^{-1})	0.69	1.31	3.22	1.45	0.67
	A (%)	16.8	29.9	26.6	14.4	12.3
29	B (T)	46.7	43.6	31.6	0.0	0.0
	δ (mm s^{-1})	0.35	0.33	0.47	0.25	0.34
	Δ (mm s^{-1})	−0.02	−0.02	−0.01	1.08	0.96
	Γ (mm s^{-1})	0.74	1.51	3.22	1.87	0.59
	A (%)	10.7	26.6	31.3	20.5	10.8

disorder in milled samples. Mössbauer spectra recorded at 295 K also show the appearance of a central doublet, which had already been noticed for S1, to a level of approximately 4% of the total spectral area. For the samples from S4 to S29, this doublet had to be fitted using two components, P1 and P2, whose hyperfine parameters vary smoothly with milling time. The isomer shifts from both doublets and magnetic sextets correspond to Fe^{3+} ions, showing that no iron reduction occurs when an open container is used during milling [19]. In addition, the relation $\Delta Q(\mathrm{P1}) > \Delta Q(\mathrm{P2})$ for the quadrupole splitting observed for all samples indicates a higher asymmetric Fe^{3+} site for P1. The quadrupole splitting for P2 remains nearly constant with milling time. The relative areas of P1 and P2 suggest that these signals might be associated with Fe^{3+} ions at the interface and in the core of $CuFe_2O_4$ nanoparticles, respectively (and/or to Fe^{3+} ions at B and A sites, respectively). Figure 4 shows the Mössbauer spectrum recorded at 295 K for the sample S29 in an applied magnetic field $H = 0.7$ T. For a ferromagnetic or ferrimagnetic material, the relative intensities of lines 2 and 5 and the relative area of the

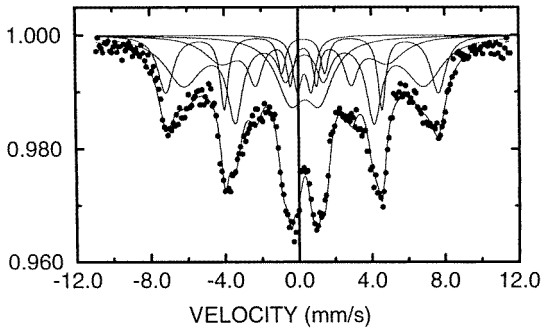

Figure 4. The Mössbauer spectrum recorded at 295 K for sample S29 with a magnetic field of 0.7 T.

magnetic component in superparamagnetic (SP) particles would increase if a magnetic field perpendicular to the gamma-ray direction was applied. Both the polarization effect and the enhancement of the sextet component can be observed for S29 (figures 3 and 4), indicating that the doublets are due to the superparamagnetic relaxation effect of nanometre-sized $CuFe_2O_4$ particles.

To further check the SP origin of the central doublets, Mössbauer measurements at 15 and 80 K were performed. At $T = 80$ K, the slowing of the SP relaxation gives fully ordered magnetic sextets, as shown in figure 5. The Mössbauer parameters obtained are displayed in

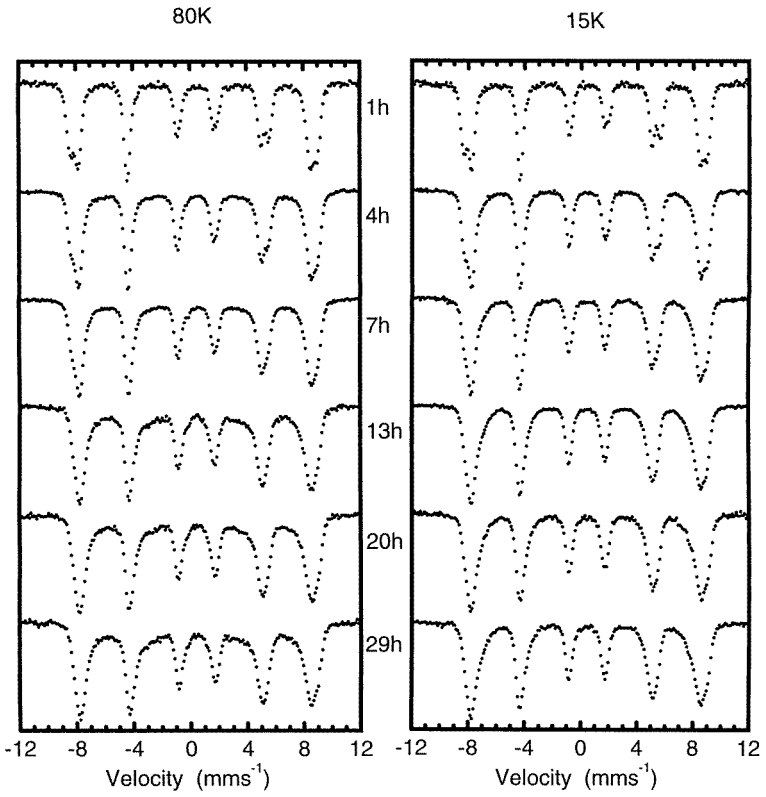

Figure 5. Mössbauer spectra recorded at 80 and 15 K for $CuFe_2O_4$ samples with various milling times.

table 2. No SP doublet is observed, while a small curvature of the baseline is noticeable. The sextet M3 with $B \approx 44$ T is observed for S4. A fourth magnetic sextet M4, with a low hyperfine field $B \approx 30$ T, was needed to fit the spectra of the samples milled for longer than 4 h. The sum of the M1 and M2 sextets from B and A sites of $CuFe_2O_4$ is only 67% of the spectral area for S29 at 80 K. Mössbauer data recorded at 15 K for $CuFe_2O_4$ samples with various milling times are also shown in figure 5. Mössbauer hyperfine parameters obtained from the fit are listed in table 3. At this temperature, the samples are well below their blocking temperatures. The sextet M4 observed at 80 K is no longer present at 15 K, and samples were fitted using three sextets (except S1 for which two sextets were needed). The hyperfine parameters of the M1 and M2 subspectra correspond to the B and A sites of $CuFe_2O_4$, in agreement with previous findings [15, 17, 18]. The M3 sextet, with a low hyperfine field and broad linewidth, might be attributed to the Fe^{3+} ions at the interface of nanostructured $CuFe_2O_4$ and/or to the Fe^{3+} ions surrounded by more vacancies (and/or Cu^{2+} ions), since the possible influence of

Table 2. Mössbauer parameters: hyperfine field (B), isomer shift (δ), quadrupole splitting (Δ), linewidth (Γ), and relative area (A), obtained by fitting the spectra recorded at 80 K for the $CuFe_2O_4$ samples milled for various times.

Milling time (h)	Parameters	M1	M2	M3	M4
1	B (T)	53.7	50.5		
	δ (mm s^{-1})	0.47	0.36		
	Δ (mm s^{-1})	−0.15	0.00		
	Γ (mm s^{-1})	0.59	0.55		
	A (%)	48.9	51.1		
4	B (T)	53.2	50.4	44.2	
	δ (mm s^{-1})	0.49	0.37	0.36	
	Δ (mm s^{-1})	−0.09	0.01	−0.17	
	Γ (mm s^{-1})	0.67	0.60	3.01	
	A (%)	43.4	44.4	12.2	
7	B (T)	52.8	50.2	45.9	30.2
	δ (mm s^{-1})	0.49	0.38	0.46	0.46
	Δ (mm s^{-1})	−0.07	0.01	−0.02	−0.13
	Γ (mm s^{-1})	0.67	0.64	2.49	3.22
	A (%)	35.2	41.1	11.5	12.1
13	B (T)	52.2	49.7	44.3	27.2
	δ (mm s^{-1})	0.48	0.37	0.50	0.50
	Δ (mm s^{-1})	−0.03	0.01	0.02	0.00
	Γ (mm s^{-1})	0.68	0.71	1.32	2.51
	A (%)	33.4	37.2	10.0	19.4
20	B (T)	52.2	49.6	44.7	29.1
	δ (mm s^{-1})	0.48	0.38	0.48	0.53
	Δ (mm s^{-1})	−0.02	0.00	0.01	0.02
	Γ (mm s^{-1})	0.68	0.72	1.62	3.22
	A (%)	34.5	34.0	12.6	19.0
29	B (T)	52.0	49.4	43.8	29.2
	δ (mm s^{-1})	0.48	0.39	0.46	0.38
	Δ (mm s^{-1})	−0.02	0.00	−0.06	−0.01
	Γ (mm s^{-1})	0.66	0.78	1.54	3.21
	A (%)	30.5	36.0	10.7	22.8

Table 3. Mössbauer parameters: hyperfine field (B), isomer shift (δ), quadrupole splitting (Δ), linewidth (Γ), and relative area (A), obtained by fitting the spectra recorded at 15 K for the $CuFe_2O_4$ samples milled for various times.

Milling time (h)	Parameters	M1	M2	M3
1	B (T)	53.7	50.4	
	δ (mm s^{-1})	0.49	0.37	
	Δ (mm s^{-1})	−0.15	0.00	
	Γ (mm s^{-1})	0.53	0.53	
	A (%)	45.8	54.2	
4	B (T)	53.4	50.5	48.1
	δ (mm s^{-1})	0.49	0.38	0.39
	Δ (mm s^{-1})	−0.10	0.01	−0.05
	Γ (mm s^{-1})	0.56	0.54	1.01
	A (%)	38.8	47.3	13.9
7	B (T)	52.8	50.3	47.0
	δ (mm s^{-1})	0.49	0.38	0.41
	Δ (mm s^{-1})	−0.05	0.01	−0.04
	Γ (mm s^{-1})	0.67	0.54	1.39
	A (%)	44.2	34.6	21.2
13	B (T)	52.6	50.1	46.5
	δ (mm s^{-1})	0.48	0.39	0.42
	Δ (mm s^{-1})	−0.02	0.00	−0.02
	Γ (mm s^{-1})	0.61	0.62	1.11
	A (%)	38.2	39.5	22.3
20	B (T)	52.6	50.0	46.1
	δ (mm s^{-1})	0.49	0.40	0.44
	Δ (mm s^{-1})	−0.02	0.00	−0.03
	Γ (mm s^{-1})	0.64	0.67	1.24
	A (%)	38.2	42.3	19.5
29	B (T)	52.4	49.8	45.9
	δ (mm s^{-1})	0.48	0.40	0.43
	Δ (mm s^{-1})	−0.01	0.00	−0.02
	Γ (mm s^{-1})	0.64	0.67	1.13
	A (%)	37.7	39.5	22.7

superparamagnetic relaxation at 15 K can be considered negligible. However, the magnetic sextets strongly overlap in the spectra recorded at 15 K, so the total average hyperfine field of $CuFe_2O_4$ versus milling time is plotted in figure 6 for further discussion. It demonstrates that the average hyperfine field of $CuFe_2O_4$ decreases rapidly with milling time up to 13 h, and then slowly saturates with further milling. A similar trend is also found for the average grain size versus milling time, as shown in figure 2.

The magnetic properties of these $CuFe_2O_4$ nanoparticles have been investigated by magnetization hysteresis curve measurements at 4.2 and 295 K, cooling the samples in a field of $H_{FC} = 80$ kOe. Figure 7 shows magnetization hysteresis curves measured at 295 K for the $CuFe_2O_4$ samples milled for various times, as an example. The corresponding parameters obtained at both temperatures are listed in table 4. It is seen that coercive force H_C and remanent magnetization M_R at room temperature decrease with increasing milling time, as a result of the increasing fraction of SP particles. On the other hand, at 4.2 K, H_C increases

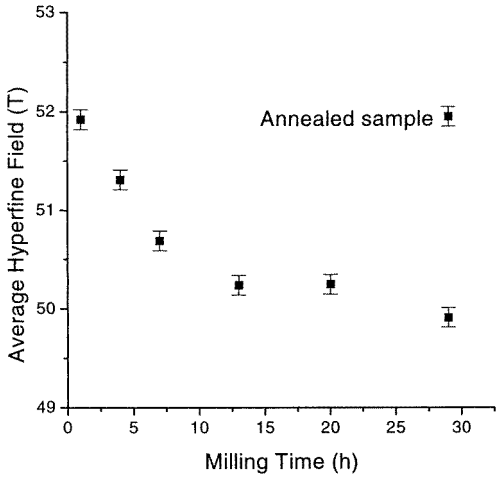

Figure 6. The average hyperfine field of iron ions in $CuFe_2O_4$ samples at 4.2 K as a function of the milling time.

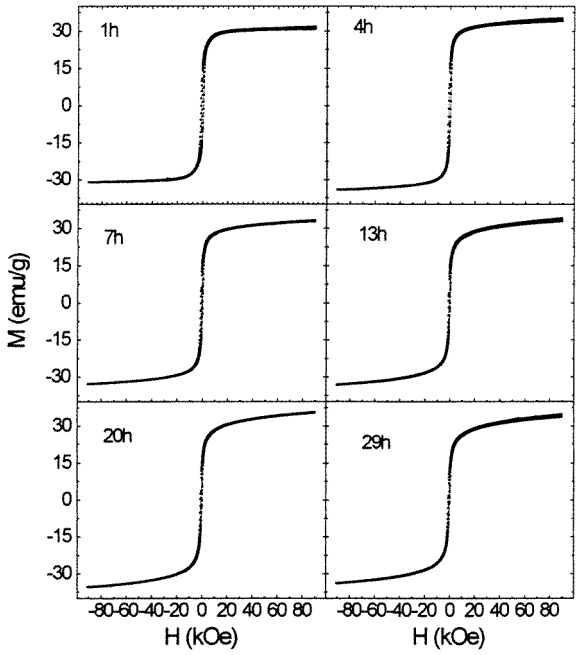

Figure 7. Magnetization hysteresis curves measured at 295 K for the $CuFe_2O_4$ samples milled for various times.

with milling time while M_R does not show a systematic change. For samples with longer milling times, the magnetization, $M(H)$, does not saturate at the maximum field attainable (90 kOe) at either temperature, and shows a marked non-linear dependence of H in the high-field region, defined as $H \geqslant 60$ kOe. In this region, the $M(H)$ curve might be described by [20] $M = M_S(1 - \alpha/H)$, where M_S is the saturated magnetization and α is a measure of the magnetic hardness of the particles. It can be seen from table 4 that the milling process initially enhances the saturation magnetization and magnetic hardness, and then they remain almost unchanged with milling time. (A similar behaviour was also found from the magnetization at 9 T, M(9 T), versus milling time.) The saturation magnetization of S29 was found to be approximately 42.2 emu g^{-1}, about 20% larger than the value 33.4 emu g^{-1} for bulk

Table 4. Magnetic parameters: coercive force, H_C, remanent induction, M_R, saturation magnetization, M_S, magnetic hardness, α, and hysteresis loop shift, ΔH, for milled $CuFe_2O_4$ samples obtained from magnetization measurements at 4.2 and 295 K. M_S and α were obtained by fitting the experimental data in the high-field region ($H \geqslant 60$ kOe) to the equation $M = M_S(1 - \alpha/H)$.

		1 h	4 h	7 h	13 h	20 h	29 h
4.2 K	M_S (emu g^{-1})	34.9(2)	39.6(2)	41.2(2)	40.8(2)	41.8(2)	42.2(2)
	α (kOe)	1.3(1)	3.9(1)	4.9(1)	6.2(1)	6.8(1)	6.8(1)
	M_R (emu g^{-1})	15.8(5)	17.0(5)	19.3(5)	16.2(5)	15.7(5)	16.0(5)
	H_C (kOe)	0.97(2)	1.04(2)	1.26(2)	1.40(2)	1.43(2)	1.56(2)
	ΔH_C (Oe)	3(5)	24(5)	130(5)	137(5)	143(5)	145(5)
295 K	M_S (emu g^{-1})	31.8(8)	35.4(8)	35.0(8)	35.6(8)	38.0(8)	37.4(8)
	α (kOe)	2.1(1)	3.6(1)	4.9(1)	6.6(1)	6.5(1)	7.0(1)
	M_R (emu g^{-1})	14.4(5)	13.0(5)	10.5(5)	8.3(5)	8.3(5)	6.3(5)
	H_C (kOe)	0.83(5)	0.72(5)	0.63(5)	0.47(5)	0.47(5)	0.38(5)

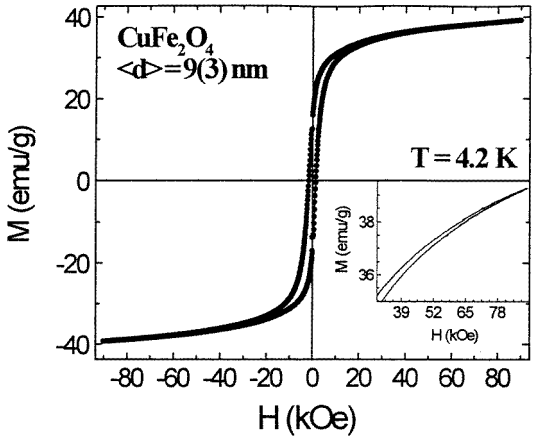

Figure 8. The magnetization hysteresis curve of the sample S29, measured at 4.2 K after field cooling with $H = 80$ kOe. The inset shows an amplified view of the high-field range of the first quadrant.

$CuFe_2O_4$ [18]. Figure 8 shows the field-cooled (FC) magnetization hysteresis loop of sample S29, taken at 4.2 K with $H_{FC} = 80$ kOe. The inset of figure 8 shows the high-field region in the first quadrant, where it can be seen that the loop remains open up to 90 kOe. This high-field magnetization irreversibility implies an anisotropy field of approximately 90 kOe, much larger than the magnetocrystalline or shape anisotropies usually observed for small particles [6, 20]. Another feature observed from field-cooled hysteresis loop measurements at 4.2 K is that the loop is not symmetrical about the origin but is shifted to the left. The shift, ΔH_C, rapidly increases from approximately 3 Oe for S1 to 130 Oe for S7 and then slowly rises to approximately 145 Oe for S29 (see table 4).

Further investigation of the magnetic properties of these nanoparticles was accomplished by studying the temperature dependence of M(9 T) and ΔH_C for sample S29. These parameters are shown in figure 9; they were taken after field cooling the sample in a field $H_{FC} = 90$ kOe. The loop shift decreases with increasing temperature and vanishes at approximately 50 K. It is also observed that ΔH_C at $T = 4.2$ K is even larger than the value obtained for S29 with $H_{FC} = 80$ kOe (see table 4). Furthermore, different slopes of M(9 T) versus temperature are clearly detected in the temperature ranges below and above approximately 50 K. These results strongly infer that a new magnetic ordering occurs below approximately 50 K in the milled sample.

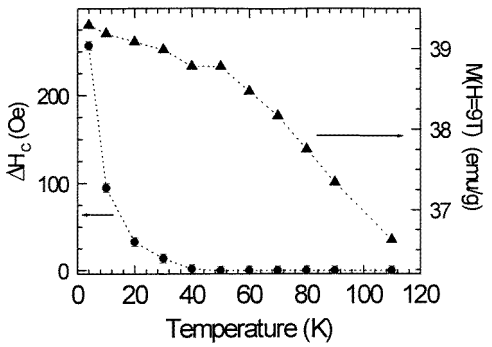

Figure 9. The hysteresis loop shift and magnetization at 9 T versus temperature for the sample S29. The loops were taken by field cooling the sample with $H_{FC} = 90$ kOe.

4. Discussion

Recently, several studies of nanometre-sized ferrites obtained by milling have found that the resulting nanoparticles are structurally and magnetically disordered due to changes in the degree of inversion, creation of oxygen vacancies, or amorphization of the structure [3, 4, 21]. However, a secondary effect of high-energy milling can be the formation of (or decomposition to) undesired phases, usually related to the reducing conditions inside a closed container. Experiments on samples of α-Fe_2O_3 (reference [22]) and α-Fe_2O_3/SiO_2 (reference [19]) powders milled in closed containers have shown that the reduction of α-Fe_2O_3 to Fe_3O_4 took place after extended milling times. The suggested mechanism implied bond breaking followed by the release of oxygen from the vial, leading to the reduction of the samples. In recent work [18], we have demonstrated that $CuFe_2O_4$ samples milled in a closed container up to 98 h pass through two stages: decomposition into α-Fe_2O_3 and CuO, and subsequent Fe^{3+}-to-Fe^{2+} reduction to form Fe_3O_4 and $Cu_xFe_{3-x}O_4$ spinels. In the present work, using an open container, neither reduction of Cu^{2+} nor reduction of Fe^{3+} were detected, which is consistent with our previous observations [19]. Since no other phases except $CuFe_2O_4$ are formed, as inferred from XRD and Mössbauer data, the properties discussed for the present system can be assigned entirely to nanometre-sized $CuFe_2O_4$ particles.

Copper ferrite is known to be magnetically soft, with values of the coercive force of about

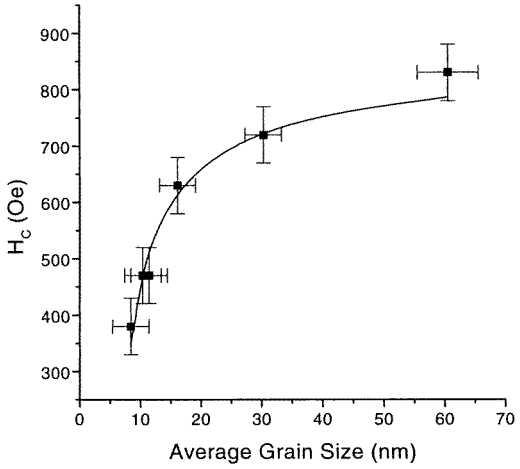

Figure 10. The room temperature coercive forces versus average grain size. The solid curve is the best fit using the equation $H_C = H_{C0}(1 - (D_P/d)^{3/2})$, where H_{C0} is the coercivity for bulk material at this temperature, from which the critical size $D_P = 6(1)$ nm and $H_{C0} = 0.8(1)$ kOe were obtained.

0.7 kOe at room temperature for bulk material [14, 18]. For particles below a critical diameter D_S, a single-domain behaviour is expected. For a given temperature, H_C decreases from its maximum value $H_C(D_S)$ to zero with decreasing particle size due to the superparamagnetic relaxation effect. The $H_C = 0$ point marks a second critical size, D_P, at which the onset of SP relaxation takes place within the magnetization measuring time ($\tau \sim 100$ s). In the $D_P \leqslant d \leqslant D_S$ region, the coercivity for an ensemble of single-domain uniaxial particles may be expressed as [20] $H_C = H_{C0}(1-(D_P/d)^{3/2})$, where H_{C0} is the coercivity of bulk material. The fit of figure 10 shows good agreement with this dependence, giving $D_P = 6(1)$ nm for the SP critical size at 295 K from the magnetization measurement and $H_{C0} = 0.8(1)$ kOe. It is worth noting that the value of H_C continues increasing up to a grain size of approximately 60 nm, indicating that $D_S \geqslant 10D_P$. At 4.2 K particles are blocked, and the magnetization will reverse by rotation since the samples that have been exposed to longer milling times are at well below their single-domain critical value D_S. The coercive force might be expressed by $H_C = 2\ K_{eff}/M_S$, where K_{eff} is related to the effective anisotropy constant. Values of K_{eff} were determined for samples after different milling times by inputting the corresponding values of H_C and M_S (table 4), and are plotted in figure 11 as a function of the average grain size. It was found that K_{eff} increases with decreasing average grain size. This reveals that the interface anisotropy gives an important contribution to K_{eff}. We analysed the results on the basis of a simple model in which the effective anisotropy is written as $K_{eff} = f_{core}K_{core}+(1-f_{core})K_{int}$, where f_{core} is the relative volume fraction of the core component, and K_{core} and K_{int} are core and interface anisotropies, respectively. Assuming that the grains are spherical with an interface thickness of t and $K_{core} = 6 \times 10^4$ erg cm^{-3} (for the bulk tetragonal $CuFe_2O_4$ in reference [23]), we found that the estimated values of K_{int} are in a range from 17×10^4 to 45×10^4 erg cm^{-3} using t-values ranging from 3 to 0.5 nm, respectively. The least-squares fit of these data yielded $K_{int} = 18(1) \times 10^4$ erg cm^{-3} and $t = 2.3(3)$ nm, and is plotted as a solid curve in figure 11. K_{int} is found to be much larger than K_{core}, which could result from a spin-disordered

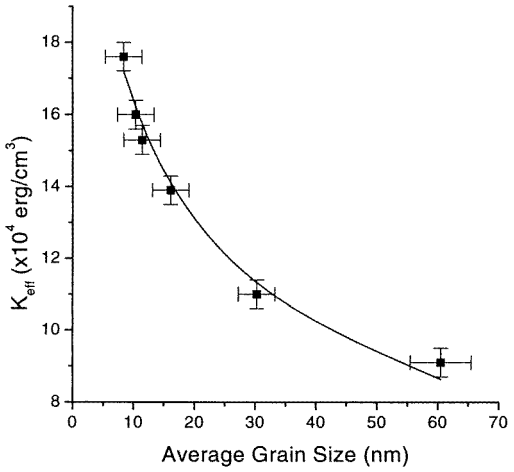

Figure 11. Effective anisotropy constants versus average grain size taken at $T = 4.2$ K. The solid curve is the best fit using the equation $K_{eff} = f_{core}K_{core} + (1 - f_{core})K_{int}$, where f_{core} is the relative volume fraction of the core component, and K_{core} and K_{int} are core and interface anisotropies, respectively, from which $K_{int} = 18(1) \times 10^4$ erg cm^{-3} and the interface thickness $t = 2.3(3)$ nm were obtained, assuming spherical grains and $K_{core} = 6 \times 10^4$ erg cm^{-3} (for the bulk tetragonal $CuFe_2O_4$ in reference [23]).

structure at the interface. From table 4, it is seen that the M_R/M_S ratio drops from about 0.46 for S1 to 0.17 for S29 at room temperature, due to the increasing fraction of superparamagnetic particles at this temperature. The M_R/M_S values for all of the samples studied at 4.2 K are slightly smaller than the expected value of 0.5 for particles with uniaxial symmetry, which could originate from interparticle interactions.

The saturation magnetization of ferromagnetic and ferrimagnetic materials usually decreases with decreasing particle size due to the existence of spin canting in most small magnetic particles. Basically, two mechanisms have been suggested to explain the origin of spin canting: one is the surface (or interface) effect [5, 6, 8–10] (hereafter model I) and the other is the finite-size effect [11–13] (hereafter model II). Variations in coordination numbers and distances of surface cations could result in a distribution of net exchange fields [6]. Competition between ferromagnetic and antiferromagnetic interactions might cause spin canting in the surface layer of magnetic particles. The surface effect, based on this argument, states that the spin structure of magnetic particles in a large applied magnetic field consists of collinear spins in a core and non-collinear spins in a surface layer (or shell). In a study on coated $NiFe_2O_4$ nanoparticles, Berkowitz *et al* [9] have suggested that organic molecules bonded to the particles act as pinning centres for the spins at the surface, giving rise to spin canting. This surface effect was later questioned by Pankhurst and Pollard [11], who suggested that spin canting in Co-doped γ-Fe_2O_3 particles might be explained by a large magnetic anisotropy energy. The doping with Co may indeed increase the magnetic anisotropy energy, but at least for pure γ-Fe_2O_3 the value of this anisotropy energy which is necessary in order to account for spin canting is much larger than the value reported for pure γ-Fe_2O_3 particles [24]. Recently, Parker *et al* [12] found that the degree of canting was identical in γ-Fe_2O_3 particles with and without a ^{57}Fe-enriched surface layer. This result, which contradicts those of earlier studies, suggests that spin canting is not a surface effect, and that it may be a finite-size effect. Very recently, Morales *et al* [13] proposed that spin canting may originate from cationic vacancy disorder within the whole particles in a study of maghemite particles. No conclusive explanation of the underlying mechanisms has yet been given [5]. Our present results show that, in copper ferrite, the saturation magnetization M_S (or magnetization at 9 T) increases with decreasing average grain size, contrary to previously reported data on other ferrimagnetic magnetic nanoparticles, e.g., $NiFe_2O_4$, for which spin canting leads to a decrease in the saturation magnetization [5–10, 12].

In inverse $MeFe_2O_4$ (Me = divalent ion) spinels, eight divalent ions are at the octahedral (B) sites and 16 trivalent (Fe^{3+}) ions are equally divided between the tetrahedral (A) and B sites per unit cell. The magnetization of sublattice A is antiparallel to that of sublattice B, whereas the magnetic moments of the ions on the A and B sublattices are ferromagnetically ordered. The total magnetic moment is entirely due to the uncompensated magnetic moments of the eight divalent ions at B sites. The magnetic moment per unit cell is $\mu = 8 \times 1\ \mu_B = 8\ \mu_B$, assuming that each divalent ion, e.g., Cu^{2+}, contributes 1 μ_B, where μ_B is the Bohr magneton. However, the energy difference between Fe occupations in A and B sites is known to be very small for Me = Cu, while it is much larger for $NiFe_2O_4$ [25]. Hence, in $CuFe_2O_4$ a cation redistribution between A and B sites could be possible. It has been observed for quenched samples that the inversion parameter δ strongly depends on the annealing temperature and cooling rate [25]. Replacing one A-site Fe^{3+} ion with a B-site Cu^{2+} ion, and vice versa, results in a magnetic moment $\mu = 7 \times 1\ \mu_B + 2 \times 5\ \mu_B - 1\ \mu_B = 16\ \mu_B$, assuming that each Fe^{3+} ion contributes 5 μ_B and a Néel-type collinear spin structure. This kind of change in cation distribution induced by milling has also been reported for other ferrites [3, 4, 26, 27]. Although the spin-canting effect observed tends to reduce M_S, the enhancement of approximately 20% of M_S for our milled $CuFe_2O_4$ samples could still be accounted for by a cation redistribution

induced during milling. From the analysis of the saturation magnetization at 4.2 K, we found that the effective magnetic moment μ_{eff} per formula unit increases from 1.5 μ_B for S1 to 1.8 μ_B for sample S29. This, in turn, may be accounted for by an increase of the degree of inversion from $\delta = 0.06$ for sample S1 to $\delta = 0.11$ for sample S29. However, inasmuch as this estimation of δ assumes fully aligned spins, it is likely that the competing effects of spin canting in these milled samples cause an underestimation of the actual δ-value.

The irreversibility observed in the $M(H)$ curves at fields of $\sim$90 kOe for the milled $CuFe_2O_4$ sample (see figure 8) implies anisotropy fields much higher than those expected for magnetocrystalline or shape anisotropy, and suggests that exchange interaction must be operative. In the following, we will discuss the high-field magnetization irreversibility, the reduction of the average hyperfine field, and the hysteresis loop shift observed in the milled $CuFe_2O_4$ samples by means of either model I or model II.

In model I, assuming that particles are composed of a ferrimagnetically ordered core and a spin-disordered surface layer, coupling between the two components is established through exchange interactions. When samples are field cooled through the ordering temperature of the spin-disordered phase, the external field will decrease the energy of some configurations of the spin-disordered phase favoured by the field direction, 'hardening' the spin reversal by rotation of the single-domain core. This could result in high-field magnetization irreversibility and a shift of the hysteresis loop. Variations in coordination numbers and distances of surface cations could reduce atomic magnetic moments on individual sublattices, resulting in lower average hyperfine fields for surface cations. Consequently, the smaller the grains, the higher the fraction of surface cations, and the lower the total average hyperfine field.

In model II, assuming the existence of spin canting in all of the particles, due to possible defects, e.g., cation site distributions and vacancies, small numbers of Cu ions occupy A sites, and the Cu(A) ions and their twelve nearest neighbours at B sites could form a cluster. Exchange coupling might arise from competing ferromagnetic (intrasublattice) and antiferromagnetic (intersublattice) interactions at the interfaces between these clusters. This coupling could also cause high-field magnetization irreversibility and hysteresis loop shift. Similar behaviours have also been reported for $ZnFe_2O_4$ (references [28–30]), lithium ferrite [31], and Ni–Mn solid solutions [32] with local fluctuations in composition. In the case of $ZnFe_2O_4$, small numbers of Fe^{3+} ions at A sites found in quenched samples or in nanostructured material form clusters with their twelve nearest neighbours at B sites, causing an enhancement of the magnetic transition temperature and saturation magnetization. In the case of Ni–Mn solid solutions, exchange anisotropy arises from competing Mn–Mn and Ni–Ni interactions at the interfaces of Ni- or Mn-rich clusters within the solution. Finally, a reduction of the average hyperfine field in milled $CuFe_2O_4$ is not unexpected, due to broken superexchange paths between Fe^{3+} ions caused by oxygen vacancies and/or Cu^{2+} nearest neighbours.

As discussed in the results section, for samples milled for longer than 7 h, Mössbauer spectra recorded at 15 K show a significant component M3 with a low hyperfine field and broad linewidth, which could be assigned to Fe^{3+} ions in locally disordered environments. It is also seen from magnetization data that the value of the magnetic hardness α increases for samples with longer milling times. It seems therefore that the effect of spin disorder is to hinder the spin reversal. The temperature dependence of ΔH_C suggests that spins freeze at approximately 50 K in the spin-disordered phase. This results in an exchange interaction between the spin-disordered phase and the rest, which shifts the magnetization loops when the sample is field cooled below the freezing temperature. Although our present data can be explained by the two-phase magnetic coupling already discussed, it cannot be ascertained at present whether the disordered phase corresponds to an actual spin-glass phase, nor whether the particles have a shell/core structure or the exchange interaction occurs between magnetic clusters within the

material. Additional measurements are required to clarify the exact mechanisms leading to the observed magnetic properties.

5. Conclusions

We have performed a study on structural and magnetic properties of copper ferrite, $CuFe_2O_4$, nanoparticles obtained from high-energy ball milling in an open container, using x-ray diffraction, Mössbauer spectroscopy, and magnetization measurements. The resulting $CuFe_2O_4$ nanoparticles show a progressive decrease of the average grain size with milling time, attaining a smallest value of $d = 9(3)$ nm. No chemical reduction effects were found. Superparamagnetic relaxation effects have been observed at room temperature by Mössbauer and magnetization measurements. At 15 K, the average hyperfine field of $CuFe_2O_4$ decreases with decreasing average grain size while the coercive force, shift of the hysteresis loop, magnetic hardness, and saturation magnetization at 4.2 K increase with decreasing average grain size. At 295 K the grain size dependence of the coercive field shows that particles are single domain, and a critical size value $D_P = 6(1)$ nm was estimated for the SP transition by means of magnetization measurements. At 4.2 K, H_C increases with decreasing grain size, which could be explained by an enhancement of the interface contribution to the effective anisotropy constant of particles. The interface anisotropy of nanostructured $CuFe_2O_4$ particles prepared by high-energy ball milling is found to be about $1.8(1) \times 10^5$ erg cm^{-3}. A cation distribution between A and B magnetic sublattices could account for the observed increase of the saturation magnetization for these particles, although spin canting was also detected. The high-field magnetization irreversibility and shift of the hysteresis loop detected for our samples have been assigned to a spin-disordered phase, which has a spin-freezing temperature of approximately 50 K.

Acknowledgments

We are indebted to A E Berkowitz, A Hernando, X Obradors, and S Mørup for fruitful discussions. Financial support from the FAPESP and the Danish Technical Research Council are gratefully acknowledged.

References

[1] See, for example,
Proc. 3rd Int. Conf. and Business Forum on Polymer Bonded Magnets (Atlanta, GA, April 1996) 1996
Proc. Int. Symp. on Ferrites (Tokyo, September 1997) 1997
Proc. 6th Int. Conf. on Ferrites (Tokyo, October 1992) 1992

[2] Koch C C 1997 *Nanostruct. Mater.* **9** 13 and references therein
Koch C C 1991 *Materials Science and Technology* vol 15, ed R W Cahn, P Hassen and E J Kramer (Weinheim: VCH) p 193
Ding J, McCormick P G and Street R 1997 *J. Magn. Magn. Mater.* **171** 309
Concas G, Congiu F and Bionducci M 1997 *J. Phys. Chem. Solids* **58** 1341

[3] Battle J, Clark T M and Evans B J 1997 *J. Physique. Coll.* IV **7** C1 257
Clark T M and Evans B J 1997 *IEEE Trans. Magn.* **33** 3745

[4] Hamdeh H H, Ho J C, Oliver S A, Willey R J, Oliver G and Busca G 1997 *J. Appl. Phys.* **81** 1851
Yermakov A 1992 *Mater. Sci. Forum* **88–90** 577

[5] Martinez B, Obradors X, Balcells L, Rouanet A and Monty C 1998 *Phys. Rev. Lett.* **80** 181

[6] Kodama R H, Berkowitz A E, McNiff E J and Foner S 1996 *Phys. Rev. Lett.* **77** 394
Parker F T, Spada F E, Cox T J and Berkowitz A E 1995 *J. Appl. Phys.* **77** 5833
Lin D, Nunez A C, Majkrzak C F and Berkowitz A E 1995 *J. Magn. Magn. Mater.* **145** 343

[7] Suber L, Zysler R, García A Santiago, Fiorani D, Angiolini M, Montone A and Dormann J L 1998 *Mater. Sci. Forum* **269–272** 937
[8] Coey J M D 1971 *Phys. Rev. Lett.* **27** 1140
Coey J M D 1987 *Can. J. Phys.* **65** 1210
[9] Berkowitz A E, Lahut J A, Jacobs I S, Levinson L M and Forester D W 1975 *Phys. Rev. Lett.* **34** 594
Berkowitz A E, Lahut J A, Jacobs I S, Levinson L M and Forester D W 1971 *AIP Conf. Proc.* **10** 966
Berkowitz A E, Lahut J A, Jacobs I S, Levinson L M and Forester D W 1980 *IEEE Trans. Magn.* **16** 184
[10] Morrish A H, Haneda K and Schurer P J 1976 *J. Physique Coll.* **37** C6 301
Haneda K and Morrish A H 1978 *Surf. Sci.* **77** 584
Ochi T, Watanabe K, Kiyama M, Shinjo T, Bando Y and Takada T 1981 *J. Phys. Soc. Japan* **50** 2777
Morrish A H and Haneda K 1981 *J. Appl. Phys.* **52** 2496
Okada T, Sekizawa H, Ambe F, Ambe S and Yamadaya T 1983 *J. Magn. Magn. Mater.* **31–34** 105
Morrish A H and Haneda K 1983 *J. Magn. Magn. Mater.* **35** 105
[11] Pankhurst Q A and Pollard R J 1991 *Phys. Rev. Lett.* **67** 248
[12] Parker F T, Foster M W, Margulies D T and Berkowitz A E 1993 *Phys. Rev.* B **47** 7885
[13] Morales M P, Serna C J, Bødker F and Mørup S 1997 *J. Phys.: Condens. Matter* **9** 5461
[14] Krupicka S and Novák P 1982 *Oxide Spinels (Ferromagnetic Materials vol 3)* ed E P Wohlfarth (Amsterdam: North-Holland)
[15] Evans B J and Hafner S 1968 *J. Phys. Chem. Solids* **29** 1573
[16] Prince E and Treuting R G 1956 *Acta Crystallogr.* **9** 1025
[17] Greenwood N N and Gibb T C 1971 *Mössbauer Spectroscopy* (London: Chapman and Hall) p 258
[18] Goya G F, Rechenberg H R and Jiang J Z 1998 *J. Appl. Phys.* **84** 1101
[19] Jiang J Z, Zhou Y X, Mørup S and Koch C B 1996 *Nanostruct. Mater.* **7** 401
[20] Cullity B D 1972 *Introduction to Magnetic Materials* (New York: Addison-Wesley)
[21] Nicoara G, Fratiloiu D, Nogues M, Dormann J L and Vasiliu F 1997 *Mater. Sci. Forum* **235–238** 145
Zhang X X, Hernandez J M, Tejada J and Ziolo R F 1996 *Phys. Rev.* B **54** 4101
Kaczmarek W A, Idzikowski B and Muller K H 1998 *J. Magn. Magn. Mater.* **177** 921
[22] Linderoth S, Jiang J Z and Mørup S 1997 *Mater. Sci. Forum* **235–238** 205
Campbell S J, Kaczmarek W A and Wang G M 1995 *Nanostruct. Mater.* **6** 735
Matteazzi P and Le Caer G 1991 *Mater. Sci. Eng.* A **149** 135
Kaczmarek W A and Ninham B W 1994 *IEEE Trans. Magn.* **30** 732
Kaczmarek W A, Onyszkiewicz I and Ninham B W 1994 *IEEE Trans. Magn.* **30** 4725
Kosmac T and Courtney T H 1992 *J. Mater. Res.* **7** 1519
[23] Kingery W D, Bowen H K and Uhlmann D R 1976 *Introduction of Ceramics* (New York: Wiley) p 993
[24] Coey J M D 1993 *J. Phys.: Condens. Matter* **5** 7297
Hendriksen P V, Linderoth S, Oxborrow C A and Mørup S 1994 *J. Phys.: Condens. Matter* **6** 3091
[25] McCurrie R A 1978 *Ferromagnetic Materials: Structure and Properties* (London: Academic) p 134
[26] Tkacova K, Sepelak V, Stevulova N and Boldyrev V V 1996 *J. Solid State Chem.* **123** 100
Sepelak V, Steinike U, Uecker D Chr, Wissmann S and Becker K D 1998 *J. Solid State Chem.* **135** 52
Sepelak V, Tkacova K, Boldyrev V V, Wissmann S and Becker K D 1997 *Physica* B **234–236** 617
[27] Arcos D, Rangavittal N, Vazquez M and Vallet-Regi M 1998 *Mater. Sci. Forum* **269–272** 87
[28] Sato T, Haneda K, Seki M and Iijima T 1987 *Proc. Int. Symp. on the Physics of Magnetic Materials* (Singapore: World Scientific) p 210
Sato T, Haneda K, Seki M and Iijima T 1990 *Appl. Phys.* A **50** 13
Kamiyama T, Haneda K, Sato T, Ikeda S and Asano H 1992 *Solid State Commun.* **81** 563
Jeyadevan B, Tohji K and Nakatshuka K 1994 *J. Appl. Phys.* **76** 6325
[29] Jiang J Z, Wynn P, Mørup S, Okada T and Berry F J 1999 *Nanostruct. Mater.* at press
[30] Schiessl W, Potzel W, Karzel H, Steiner M, Kalvius G M, Martin A, Krause M K, Halevy I, Gal J, Schafer W, Will G, Hillberg M and Wappling R 1996 *Phys. Rev.* B **53** 9143
[31] Dormann J L, El Harfaoui M, Nogues M and Jove J 1987 *J. Phys.: Condens. Matter* **20** L161
Nogues M, Villers G, Dormann J L and Teillet J 1990 *IEEE Trans. Magn.* **26** 2229
[32] Kouvel J S, Graham C D and Jacobs I S 1959 *J. Physique Radium* **20** 198
Meiklejohn W K 1962 *J. Appl. Phys.* **33** 1328